RESEARCH ARTICLE
doi: 10.2306/scienceasia1513-1874.2025.s017

ScienceAsia 51S (2): 2025: ID 2025s017: **1–11**

Enhanced mechanical, electrical, and *in vitro* apatite-forming ability of the nano-hydroxyapatite bioceramics via $Bi_{0.50}(Na_{0.80}K_{0.20})_{0.5}TiO_3$ addition

Pharatree Jaita[a,b,c], Pimpilai Wannasut[a,b,c], Orawan Khamman[a,b], Anucha Watcharapasorn[a,b], Parkpoom Jarupoom[d,e,*]

[a] Department of Physics and Materials Science, Faculty of Science, Chiang Mai University, Chiang Mai 50200 Thailand
[b] Center of Excellence in Materials Science and Technology, Materials Science Research Center, Faculty of Science, Chiang Mai University, Chiang Mai 50200 Thailand
[c] Office of Research Administration, Chiang Mai University, Chiang Mai 50200 Thailand
[d] Department of Industrial Engineering, Faculty of Engineering, Rajamangala University of Technology Lanna (RMUTL), Chiang Mai 50300 Thailand
[e] Materials and Medical Innovation Research Unit, Faculty of Engineering, Rajamangala University of Technology Lanna (RMUTL), Chiang Mai 50300 Thailand

*Corresponding author, e-mail: noteparkpoom@gmail.com

Received 18 Nov 2024, Accepted 1 Jul 2025
Available online 18 Aug 2025

ABSTRACT: In this research, the bioceramics system of nano-hydroxyapatite-bismuth sodium potassium titanate or $Ca_{10}(PO_4)_6(OH)_2/xBi_{0.50}(Na_{0.80}K_{0.20})_{0.5}TiO_3$ (HAp/xBNKT), where x = 0, 20, 40, and 60 wt% were fabricated by a solid-state mixed oxide technique. The HAp powder was synthesized from bovine bone, which is a natural material and a waste product. The effect of BNKT concentration on phase evolution, physical, microstructure, mechanical (i.e., Vickers hardness (HV), Knoop hardness (HK), and fracture toughness (K_{IC})), dielectric, ferroelectric, and piezoelectric properties as well as *in vitro* apatite-forming ability of the HAp bioceramic have been systematically investigated. XRD revealed that pure HAp bioceramic had a hexagonal phase while the modified compositions showed two-phase mixture of HAp and BNKT. With increasing BNKT content, the prepared HAp/xBNKT bioceramics exhibited more dense structure and increased linear shrinkage value. Adding more BNKT also inhibited grain growth and resulted in improving mechanical and electrical performances. The maximum values of mechanical (HV = 5.49 GPa, HK = 5.28 GPa, K_{IC} = 6.90 MPa.m$^{1/2}$), dielectric (ε_r = 230.28, $\tan\delta$ = 0.0728, ε_{max}= 443.33), ferroelectric (P_{max} = 25.46 μC/cm^2, P_r = 18.99 μC/cm^2, E_c = 10.08 kV/cm), and piezoelectric (d_{33} = 66 pC/N) properties were observed for the HAp/60BNKT bioceramics. For *in vitro* bioactivity test, all HAp/xBNKT bioceramics showed a good apatite-forming ability to induce apatite precipitation in a simulated body fluid solution. The results indicated that the HAp/60BNKT bioceramics had potential to exhibit excellent mechanical and electrical performances with good bioactivity, and thus being a promising biomedical application material.

KEYWORDS: nano-hydroxyapatite bioceramic, bismuth sodium potassium titanate ceramic, mechanical properties, electrical performances, *in vitro* apatite-forming ability

INTRODUCTION

Bioceramic is a group of biological materials widely used in biomedical applications to replace or regenerate the damaged bone or muscular tissues in human skeletal system [1]. Among various forms of the bioceramics, hydroxyapatite or HAp has gained great extensive studies [1, 2]. HAp is a biomaterial calcium phosphate crystal that plays a vital role in bone grafting and particularly generating new form of crystals in the existing bone [3]. The formula of HAp is $Ca_{10}(PO_4)_6(OH)_2$ [4] and it has chemical/structural similarities to the mineral phase of hard tissues [3, 5]. The HAp can also be found in compounds such as bone, hard tissue and dental enamel as well as proteins and other organic materials [6]. Several synthesis methods have been described to produce HAp; (1) synthesis from various natural resources, i.e. natural bovine bone, chicken bone, fish bone, and egg-shells [7]; (2) synthesis in laboratory using mineral-based chemicals, i.e. combustion, solid-state reaction, hydrothermal emulsion, sputtering, precipitation, biomimetic deposition, electrodeposition, wet chemical precipitation reaction, and sol-gel methods [8, 9]. The HAp is biodegradable with low-toxicity, good osteoconductive and osteoinductive capabilities, long-term stability in the living tissues, and excellent biocompatibility with hard tissues/skin/muscle tissues [10, 11]. However, the poor mechanical (i.e. low toughness and brittleness) and poor electrical properties have necessitated the development of HAp-based composites with various compounds [11]. The electrical properties of human bone are also essential to their healing and remodeling [12].

In order to improve the mechanical and electrical performances of HAp bioceramic, many researchers are much interested in HAp-based composites with the piezoelectric materials, such as $Ba_{0.96}Ca_{0.04}TiO_3$ (BCT)

[12], $BaTiO_3$ (BT) [13, 14], $Na_{0.5}K_{0.5}NbO_3$ (NKN) [15], $CaTiO_3$ (CT) [16], for bone repair and bone regeneration because of their ability to imitate the electrical properties of natural bones [12]. Piezoelectric materials are a class of materials that develop an electrical polarization when strained through applied stress [17]. These materials have significant applications in tissue engineering as an electro-active scaffold for tissue regeneration. Furthermore, the piezoelectric materials may also promote cellular development and differentiation by simulating the electric potential created by stress in tissues like bone and cartilage [18]. Bowen et al [13] studied the relationships between composition and electrical properties (i.e. dielectric and piezoelectric) of the hydroxyapatite-barium titanate composites ($HAp/BaTiO_3$) for polarized bone substitutes. They found that the addition of $BaTiO_3$ into HAp led to an increase in dielectric constant (ε_r) and AC conductivity. Ibrahim et al [12] studied the HAp-$Ba_{0.96}Ca_{0.04}TiO_3$ or HAp-BCT composites. They found that the grain boundary resistivity was higher in comparison to the resistivity exhibited inside the grains. This demonstrated the distinct electrical conductivity at the interfaces between the grains in comparison to the interior of the grains. The mechanical analysis indicated that the average hardness ranges from 4.77–5.22 GPa. The data suggest that these HAp-BCT composites may have the potential to be a biomedically helpful substance. The incorporation of varying amounts of piezoelectric biocompatible $Na_{0.5}K_{0.5}NbO_3$ (NKN) on dielectric and electrical properties of HAp was also investigated by Verma et al [15]. The dielectric and electrical responses of the HAp can be enhanced by the incorporation of biocompatible piezoelectric NKN secondary phase to achieve bone-like electrical properties. The ε_r and AC conductivity of the fabricated composites are almost equivalent to the human bone. Overall, the HAp-xNKN system can be suggested as a potential material for electro-active orthopedic implant applications.

Among various piezoelectric ceramics, bismuth sodium potassium titanate, $Bi_{0.5}(Na_{1-x}K_x)_{0.5}TiO_3$ or $BNKT_x$ ceramics have been extensively studied and suggested as a promising candidate for piezoelectric applications. Sasaki et al [19] found that $BNKT_x$ ceramics exhibited the morphotropic phase boundary (MPB) between rhombohedral (R) and tetragonal (T) phases near $x = 0.16$–0.20 [20]. The electrical properties enhancement of $BNKT_x$ ceramics over this MPB region was similar to that observed for $Pb(Zr,Ti)O_3$ or PZT ceramics. The composition of $Bi_{0.50}(Na_{0.80}K_{0.20})_{0.5}TiO_3$ or $BNKT_{20}$ ($x = 0.20$) is an electrically active piezoelectric material with reasonably high dielectric constant ($\varepsilon_r \sim 1419$, $T_m \sim 320\,^{\circ}C$), good ferroelectric with high spontaneous polarization ($P_r \sim 30.48\ \mu C/cm^2$, $E_c \sim 31.49$ kV/cm), and excellent piezoelectric properties ($d_{33} \sim 178$ pC/N, $S_{max} \sim 0.23$ %, $d*_{33} \sim 418$ pm/V) at room temperature (RT) [21, 22]. This piezoelectric ceramic group has mechanically created electric surface potentials, which could be the key to functionalizing existing designs. Therefore, they can be used to simulate the bone's ability to generate electrical prospects in response to mechanical stress without needing an external power source [12].

To our knowledge, no thorough study has been done on the bioceramic system of $Ca_{10}(PO_4)_6(OH)_2/xBi_{0.50}(Na_{0.80}K_{0.20})_{0.5}TiO_3$ or HAp/xBNKT. Furthermore, the mechanical and electrical characteristics of the HAp/xBNKT bioceramics have not been described. Based on the above perspective, it would be of interest to develop the HAp/xBNKT bioceramics and assess their mechanical, electrical properties, and biocompatibility. The studied HAP powder in this work was synthesized from bovine bone, which is a natural material and a waste product. This method is easy and quick to prepare. We selected the $Bi_{0.50}(Na_{0.80}K_{0.20})_{0.5}TiO_3$ from our preliminary and many research work which indicated that this composition has excellent electrical properties (dielectric, ferroelectrics, piezoelectric) [19–22]. The addition of $Bi_{0.50}(Na_{0.80}K_{0.20})_{0.5}TiO_3$ or BNKT into the HAp matrix in an optimal amount is anticipated to improve mechanical and electrical responses of the HAp. In this work, four different HAp/xBNKT compositions with various BNKT content of 0, 20, 40, and 60 wt% were developed, and a significant effort was invested to optimize the sintering conditions. The resulting bioceramics were investigated by X-ray diffraction (XRD) and scanning electron microscopy (SEM) techniques. The Archimedes' principle was used to study the physical properties while the mechanical properties were analyzed by Vickers and Knoop microhardness. The electrical properties which include dielectric, ferroelectric, and piezoelectric were also measured. To evaluate the bioactivity interaction, all HAp/xBNKT bioceramics were immersed in simulated body fluid solution (SBF) for 21 days to check *in-vitro* apatite-forming ability test by applying SEM technique. We expected that these bioceramic system would possess good mechanical and electrical performances with excellent bioactivity when compared to other previous studies [12–15], suggesting their potential to use for biomedical applications.

MATERIALS AND METHODS

The nano-hydroxyapatite powder, $Ca_{10}(PO_4)_6(OH)_2$ or nano-HAp was derived from the natural bovine bone by a sequence of thermal processing. First, the fresh bovine bones of a cow were defatted by boiling in distilled water to remove the tendons for 8 h. The boiled bones were then dried at 200 °C overnight. After that, the deproteinized bone was calcined at 800 °C for 3 h dwell time with a heating/cooling rate of 3 °C/min. To obtain the nano-powder, the HAp was then milled

by applying a high-energy vibro-milling method for 20 min. This process was detailed in our previous works [7, 23]. Lead-free $Bi_{0.50}(Na_{0.80}K_{0.20})_{0.5}TiO_3$ or BNKT powder was synthesized by a solid-state reaction method. The analytical grade reagents of metal oxide powders, including Bi_2O_3 (99.9%), Na_2CO_3 (99.5%), K_2CO_3 (99%), and TiO_2 (99.9%), were used as starting materials. All hygroscopic powders were first dried at 120 °C for 24 h in order to remove the residual moisture. The raw materials of BNKT powder were stoichiometrically weighed, ball-milled in high-purity ethanol solution (99.9%) for 24 h and dried in an oven at 120 °C overnight. The BNKT powder was calcined in a closed Al_2O_3 crucible at 900 °C for 2 h with a heating/cooling rate of 5 °C/min [21, 22].

The calcined nano-HAp and BNKT powders were stoichiometrically weighted, and ball-milled again in 99.9% ethanol solution for 24 h using stabilized zirconia milling media to produce the mixed powder of HAp/xBNKT, where x = 0, 20, 40, and 60 wt%, respectively. After that, the mixed HAp/xBNKT powders were dried using the oven-dried technique at 120 °C for 24 h. To prepare the HAp/xBNKT bioceramics, a few drops of 4 wt% polyvinyl alcohol (PVA) binders were added to the mixed HAp/xBNKT powders before being uniaxially pressed into discs 10 mm in diameter with a thickness of 1.3 mm. These green pellets were embedded into the powder of the same composition to minimize the loss of the volatile elements and were then sintered at an optimum sintering temperature of 1250 °C for 2 h with a heating/cooling rate of 3 °C/min in a covered alumina crucible. All sintered HAp/xBNKT bioceramics were then subjected to properties characterization.

Phase analysis of both powders and ceramics was characterized using an X-ray diffractometer (XRD, Rigaku, MiniFlex 600, Tokyo, Japan) with CuKα radiation. Survey shooting was carried out in the range of reflection angles 2θ = 20°–80° with a step of 0.02°/s and λ of 1.5406 Å. The bulk density was measured in accordance with Archimedes' method. The linear shrinkage (S_L) was calculated using the following empirical equation: $S_L = [(D_1 - D_2)/D_1] \times 100\%$, where D_1 (mm) is the length of the mold, and D_2 (mm) is the length of the sample after the complete sintered. The porosity of all ceramics was also determined based on the ASTM C830 standard [23]. The dried samples were weighed and saturated with water (a liquid that wet the sample). Then the test sample was weighed in a saturating liquid, and the pore volume was determined from the difference in the sample mass in liquid and in air. The as-sintered surface and fracture surface modes of all HAp/xBNKT bioceramics were imaged using a scanning electron microscope (SEM, JEOL JSM-6335F, Tokyo, Japan). The grain size was determined by a mean linear interception method from SEM micrographs (ASTM E112-88) [22]. For mechanical properties measurement, all HAp/xBNKT bioceramics were polished to a mirror-finished. The well-polished samples were then subjected to the microhardness tester of both Vickers hardness (HV) and Knoop (HK) determinations. The indentation load used was 1000 N which was applied for 15 s holding time. Fracture toughness (K_{IC}) was also determined from cracks' length propagated from four corners of indentation impression following the method described by Anstis et al [24].

For electrical characterization, all HAp/xBNKT bioceramics were carefully polished to 1 mm thickness to obtain parallel scratch-free surfaces. The top and bottom electrodes were made by coating silver paint on both sides of the polished sample disks, followed by annealing at 600 °C for 20 min. The temperature dependence of the dielectric properties was measured using an LCR-meter over a temperature range of 25–500 °C at various frequencies of 10, 100, and 500 kHz. The ferroelectric properties were investigated by a Radiant Precision ferroelectric tester (Precision Premier II, Radiant Technologies, Albuquerque, NM, USA) at room temperature (RT). An AC electric field of 20 kV/cm at a frequency of 1 Hz was utilized in the hysteresis loop measurement. The maximum polarization (P_{max}), remnant polarization (P_r), and coercive field (E_c) values were determined from the polarization-electric field (P-E) hysteresis loops. For piezoelectric measurements, all bioceramics were poled for 15 min at RT with an applied DC electric field of 2 kV/mm in a stirred silicone oil bath. The piezoelectric coefficient (d_{33}) was then recorded for the 24 h aged sample at a frequency of 50 Hz using a d_{33}-meter. For *in-vitro* apatite-forming ability or bioactivity test, all HAp/xBNKT bioceramics were immersed in the SBF solution. All bioceramics were limited to 1 cm^2 of the active area and were immersed for 21 days in falcon tubes containing 40 ml of SBF solution at 37 °C in a water bath. The SBF solution was changed every 1 h for up to 12 h, followed by replacement with fresh solution once a day for 21 days. Afterwards, all bioceramics were removed from the fluid and the surfaces were investigated by SEM techniques. The ionic concentration of SBF (in mM) used was as follows: Na^+ = 142.0, K^+ = 5.0, Ca^{2+} = 2.5, Mg^{2+} = 1.5, Cl^- = 148.8, HCO_3^- = 4.2, HPO_4^{2-} = 1.0, SO_4^{2-} = 0.5 [23].

RESULTS AND DISCUSSION

Phase evolution and densification

X-ray diffraction patterns of the HAp/xBNKT bioceramics, where 2θ = 20°–80° are shown in Fig. 1(a). No reaction products between two phases of HAp and BNKT were observed. All samples had no detectable impurities or secondary peaks. The HAp bioceramic had a hexagonal phase in which OH^- ions are placed at centroid of the triangle formed by Ca^{2+} ions along the longitudinal axis of hexagonal unit cell together with tetrahedral phosphate (PO_4^{3-}) ions [15]. This was

Table 1 Physical, microstructure, and mechanical properties of the HAp/xBNKT bioceramics.

x (wt%)	Density (g/cm^3)	Relative density (%)	Linear shrinkage (%)	Porosity (%)	Grain size (μm)	HV (GPa)	HK (GPa)	K_{IC} (MPa.m$^{1/2}$)
0	2.79	95.87	13.75	1.99	2.32	3.04	2.89	0.99
20	3.11	96.14	16.12	1.47	2.13	3.59	3.31	1.43
40	3.52	96.69	22.92	0.88	1.61	4.79	4.46	4.46
60	4.08	98.01	24.93	0.61	1.36	5.49	5.28	6.90

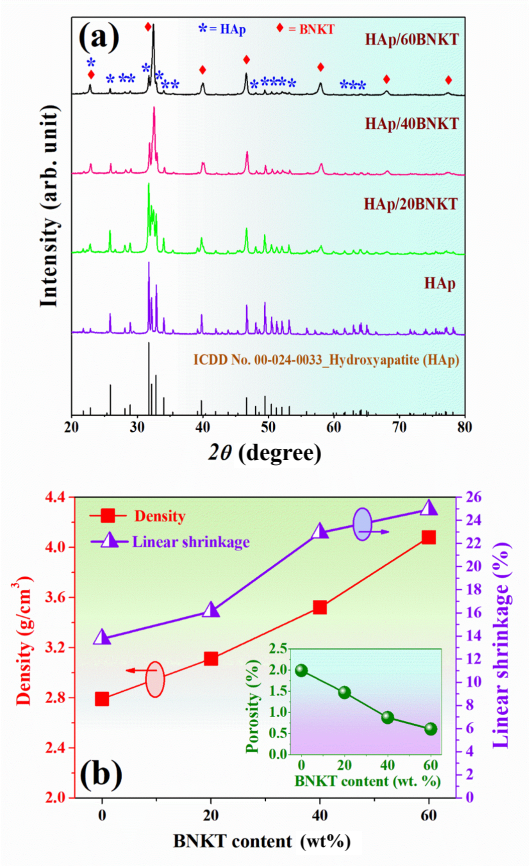

Fig. 1 (a) X-ray diffraction patterns of the HAp/xBNKT bioceramics, where 2θ = 20°–80° and (b) plots of density and linear shrinkage values as a function of BNKT content (inset: porosity value as a function of BNKT content).

correlated with ICDD data file no. 00-024-0033 and in agreement with the stoichiometric of the HAp in many previous works [7, 23, 25]. By increasing the BNKT content to 20 wt%, the main peaks of HAp phase (marked as "*") were observed, while the intensity of BNKT phase (marked as "♦") was very low. With increasing BNKT content up to 40–60 wt%, the intensity of BNKT phase was more apparent. Except for the pure HAp bioceramic, all modified compositions showed two-phase mixture peaks of HAp and BNKT with intensities corresponding to the relative amount of each phase.

The densification of all HAp/xBNKT bioceramics sintered at 1250 °C for 2 h dwell time was investigated using Archimedes' method. Plots of the bulk density as a function of BNKT content of the HAp/xBNKT bioceramics are shown in Fig. 1(b). The data clearly shows that the variation of BNKT concentration significantly influenced the density value. The density of pure HAp bioceramic was found to be 2.79 g/cm^3, which was close to 2.86–2.91 g/cm^3 observed earlier by Jaita et al [7] and Jarupoom et al [25]. The density value for this HAp bioceramic was higher when compared to that of the previous work for the compact bone mineral density of the normal human (∼1.147–1.179 g/cm^3, age groups 30–39 years) [26]. The density increased with increasing BNKT content and reached a maximum value of 4.08 g/cm^3 for the HAp/60BNKT bioceramic (Table 1). The relative density (∼95.87–98.01%) also showed similar trend to that of the bulk density value. It can be seen that the addition of BNKT into HAp bioceramic caused an increase in samples' density. This result was also correlated with increasing of the linear shrinkage value and decreasing of the porosity value with increasing BNKT additive, as also shown in Fig. 1(b). The maximum linear shrinkage of 24.93 % was also obtained for the HAp/60BNKT bioceramic. These results suggested that the HAp/60BNKT bioceramic had the highest density and hence lowest porosity value. This result was also consistent with the previous work studied by Mohammad et al [27]. They also reported that sintering of bioceramic sample made of the pure shell of *Anadara granosa* or Malaysian cockle promoted the densification. When the porosity of sample decreased, the density of all samples would increase as expected. The reason for the increasing trend of the measured density should be linked with the fact that the BNKT ceramic has a higher density (∼5.84 g/cm^3) [28] than the pure HAp bioceramic (∼2.91 g/cm^3) [25].

Microstructure and mechanical properties

In this section, the SEM was used to determine the morphologies of as-sintered surface and fracture surface modes of all bioceramics. The SEM micrographs with as-sintered surface are shown in Fig. 2(a–d). Grain size value was measured and calculated based on a mean linear intercept method. This method was the quantitative measurement of grain size within dense uniform structures and it was best suited where the boundaries of each grain were relatively easy to de-

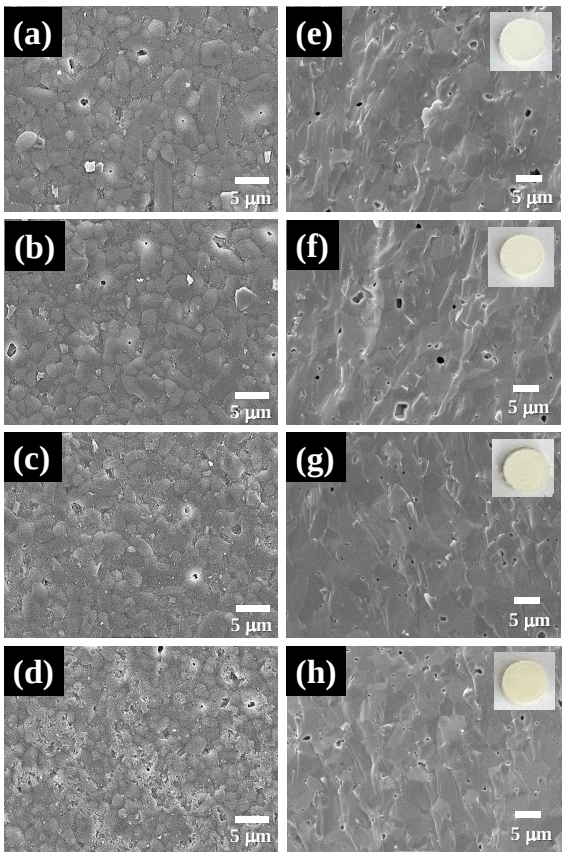

Fig. 2 SEM micrographs and their products after sintering process of the HAp/xBNKT bioceramics, (a–d) as sintered surface mode and (e–h) as fracture surface mode for the x = 0, 20, 40, and 60 wt% BNKT bioceramics, respectively.

termine [21]. It can be seen that all bioceramics were good sintered, dense with well-developed microstructure and relative density higher than 95% of their theoretical density. The regular grain boundaries and equiaxed grain shape were clearly present in all samples. Conversely, the addition of BNKT into the HAp resulted in an obvious change in the average grain size value, which is also summarized in Table 1. Microstructural analysis indicated that increasing BNKT content decreased the average grain size value. This grain size value decreased from 2.32 µm for the pure HAp bioceramic to around 2.13 µm for higher amounts of added BNKT (x = 20 wt%), and then slightly decreased to a minimum value of around 1.36 µm for the HAp/60BNKT bioceramic. Therefore, the grain size of this studied bioceramics could be controlled by the BNKT addition. We believe that the slightly reduced average grain size for this system was due to the fact that most of the BNKT added dopants were incorporated only at the grain boundary region, and this decreased the actual effective concentration inside the grain [29] and finally caused the reduction of grain

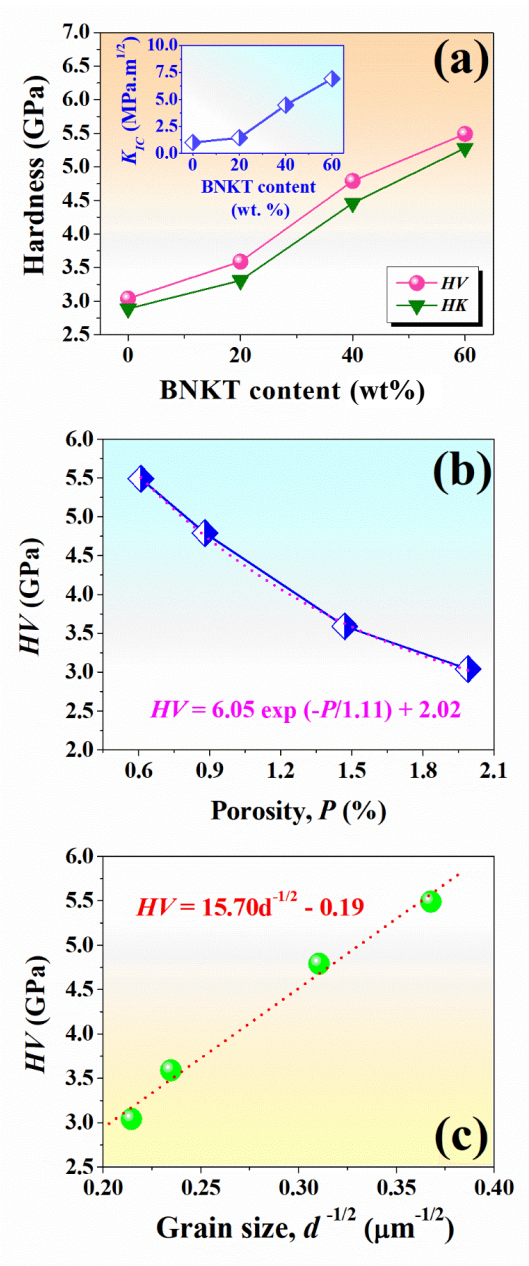

Fig. 3 (a) Plots of HV and HK values as a function of BNKT content of the HAp/xBNKT bioceramics (inset: K_{IC} value as a function of BNKT content), (b) plots of (a) HV as a function of porosity (P), and (c) HV as a function of average grain size ($d^{-1/2}$) of the HAp/xBNKT bioceramics.

size. The fracture surfaces of all samples and their products after sintering process are also presented in Fig. 2(e–h). The fracture surface of the pure HAp bioceramic displayed coarser grain with intra granular cleavage and showed predominantly porous structure. By increasing BNKT content to 20–60 wt%, the SEM images showed a finer grain with intra granular and

denser microstructure. This result also agrees well with the measured density result, i.e. the density increased while the porosity decreased with increasing BNKT content [27].

Mechanical characteristic of the HAp/xBNKT bioceramics in terms of HV and HK hardness were investigated and the values are summarized in Table 1. The HV and HK values were determined using following equations [7, 16, 30, 31]:

$$HV = 1.8544\ \frac{P}{d^2}, \tag{1}$$

$$HK = 14.229\ \frac{P}{L^2}, \tag{2}$$

where P = applied load (N), d = average size of the measured diagonals of the indentation impression (mm), and L is the measured long diagonal of the residual impression (mm). In addition, K_{IC} was also calculated in this research work by using the following equation [32]:

$$K_{IC} = 0.0016\ \frac{P}{C^{3/2}}\left(\frac{E}{H}\right)^{1/2}, \tag{3}$$

where P is the load (N), C is the crack length from the center of the indent to the crack tip (m), E is the Young's modulus (GPa), and H is the Vickers hardness (GPa). Plots of HV and HK values as a function of BNKT content are shown in Fig. 3(a). The HV and HK values of the pure HAp bioceramic were 3.04 GPa and 2.89 GPa, respectively. The hardness value for this HAp bioceramic was higher when compared to that of the previous work for mechanical properties of bones using micro and nanoscale tests for the human femoral osteonal and interstitial lamellae, which had the hardness of between 0.51 and 0.8 GPa (for lamelar human bone) [33, 34]. It can be seen that the hardness value of the HAp bioceramic was improved by adding BNKT content. The HV and HK values initially increased with increasing the BNKT additive, and then reached the maximum value of 5.49 GPa and 5.28 GPa, respectively, for the HAp/60BNKT bioceramic. The hardness value for this composition was slight higher when compared to that of the previous work for the HA-BCT ceramics, which had the hardness of ∼4.77–5.02 GPa [12]. The K_{IC} studied was shown in the inset of Fig. 3(a). It was found that the K_{IC} value also increased with increasing BNKT additive content. The maximum K_{IC} of 6.90 MPa.m$^{1/2}$ was also obtained for the HAp/60BNKT bioceramic. The mechanical improvement of the HAp/xBNKT bioceramics over of the unmodified samples was partly contributed to the combination of densification improvement and the reduction of grain size as can be seen from the SEM micrographs in Fig. 2, which can give rise to better mechanical performances [35]. The average grain size influenced the mechanical properties and the grain boundaries act as a barrier to dislocation motion for two reasons: (1) because the two grains are different in orientation, a dislocation passing into the next grain must change its direction of motion, and this becomes more difficult as the crystallographic misorientation increased and (2) the atomic disorder within grain boundary region resulted in a discontinuity of slip planes from one grain to another. Hence, the samples having smaller grain size contained more grain boundaries, which restricted crack motion, leading to higher hardness and stronger materials [25, 36]. Furthermore, the ceramics with smaller grain size could possess single domain state and caused the generation of the residual stress during sintering, which could not be released. Therefore, this would lead to the improvement of the apparent K_{IC} value [36].

The porosity (P) of the bioceramics also affected the measured hardness value. It has been proposed that the relation between HV and P for many ceramics can be expressed as the following equation [37]:

$$HV = H_0 \exp(-bP), \tag{4}$$

where HV is the measured Vickers hardness, H_0 is Vickers hardness value corresponding to a specimen with zero porosity or the hardness of completely dense material, b is a material dependent constant, and P is the volume fraction porosity of the specimen. Plots of HV as a function of P is shown in Fig. 3(b) which demonstrated that the mechanism of decreasing hardness value with porosity in an exponential fashion is related to the fact that fracture is more likely to occur as porosity increased. In this work, the relation between the HV had an exponential relation with first order of P value and can be expressed as: $HV = 6.05\exp(-P/1.11)+2.02$. As expected, a lower porosity volume fraction can resulted to higher HV value [7].

In some ceramics, the relationship between Vickers hardness and grain size (d) can follow the Hall-Patch equation [38, 39]:

$$HV = H_0 + kd^{-1/2}, \tag{5}$$

where HV is Vickers hardness, k and H_0 are constants, and d is grain size. Plots of HV as a function of grain size ($d^{-1/2}$) is presented in Fig. 3(c). It was found that the HV data for the studied bioceramics obeyed the Hall-Petch relation, where the HV value increased with a decrease of the average grain size and can be expressed as: $HV = 15.70d^{-1/2} - 0.19$. The density increased while the porosity and the average grain size decreased with increasing BNKT concentration. These factors may contribute to an improvement of both hardness and fracture toughness values of the studied bioceramics.

Dielectric analysis

Dielectric constant is a characteristic parameter of a dielectric material which determines the extent of the

Table 2 Dielectric, ferroelectric, and piezoelectric properties of the HAp/xBNKT bioceramics.

x (wt%)	ε_r [a]	$\tan\delta$ [a]	ε_{max} [b]	P_{max} ($\mu C/cm^2$)	P_r ($\mu C/cm^2$)	E_c (kV/cm)	d_{33} (pC/N)
0	31.73	0.0151	36.28	1.22	0.43	5.35	10
20	55.31	0.0177	62.25	1.64	1.47	9.30	22
40	63.76	0.0320	90.57	1.91	1.64	9.38	34
60	230.28	0.0728	443.33	25.46	18.99	10.08	66

[a] = dielectric data at room temperature, measured at 10 kHz. [b] = dielectric data at maximum temperature, measured at 10 kHz.

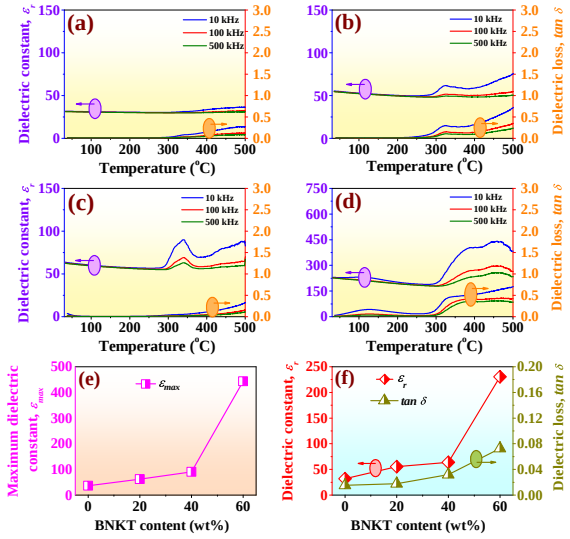

Fig. 4 Dielectric constant (ε_r) and dielectric loss ($\tan\delta$) as a function of temperature of the HAp/xBNKT bioceramics, (a) HAp, (b) HAp/20BNKT, (c) HAp/40BNKT, (d) HAp/60BNKT, (e) the ε_{max} as a function of BNKT content, and (f) the ε_r and $\tan\delta$ as a function of BNKT content.

polarizability existing under the applied alternating current [40]. Dielectric constant (ε_r) and dielectric loss ($\tan\delta$) as a function of temperature of the HAp/xBNKT bioceramics measured at different frequencies from 10–500 kHz are shown in Fig. 4(a–d). The related dielectric values are also listed in Table 2. It was observed that the ε_r of all HAp/xBNKT bioceramics increased with increasing temperature at the given frequencies (10–500 kHz). As the temperature was raised, the value of the ε_r raised because of an increase in the number of charge carriers [12]. The variation of ε_r with temperature was due to relaxation of space charge and dipolar polarization [15, 40]. However, an increase of ε_r with temperature is much more significant at lower frequencies than at higher frequencies. This may be due to the development of interfacial polarization in the presence of two phases with distinct weight percentages and electrical conductivity [12, 15, 41]. Changes in the electrical field at a low frequency lead to all polarizations. With increasing frequency, some polarizations, especially interfacial polarizations cannot happen following the change of the electric field due to lengthy time for the construction of space charge polarization. Therefore, the ε_r is lower at high frequency. The ε_r value decreased with increase in frequency and the high frequency plateau is weakly dependent on the temperature [41]. For the dielectric loss, the $\tan\delta$ also increased in tandem with the temperature. The $\tan\delta$ exhibited larger value in the lower and intermediate frequency zones. The vibrations of ions may become ion jump and conduction loss caused by ion migration, in addition to the phenomenon of ionic polarization occur. In the higher frequency range, the vibrations of ions may become the only contributor to the loss tangent, resulting in a reduction in $\tan\delta$ within this higher frequency band [12].

Based on Fig. 4(a–d), it can be seen that the dielectric curve of the pure HAp bioceramic presented less stability as compared to other samples, i.e. it showed flat curve at all temperatures and all frequencies. However, the dielectric curve of the modified bioceramics (i.e. HAp/20BNKT, HAp/40BNKT, and HAp/60BNKT) exhibited a good dielectric constant-temperature curve. This was due to the fact that the dielectric constant-temperature curve of the BNKT phase had peaks at its transition temperatures [21, 22]. Based on Table 2, it was found that the ε_{max} at a frequency of 10 kHz increased with increasing BNKT content and reached a maximum value of 443.33 for the HAp/60BNKT bioceramic (Fig. 4(e)). Data of dielectric performance at RT and a frequency of 10 kHz is also displayed in Fig. 4(f). The HAp bioceramic had ε_r and $\tan\delta$ of 31.73 and 0.0151, respectively. As it was expected, the measured ε_r and $\tan\delta$ increased with increasing BNKT concentration and showed the maximum values of 230.28 and 0.0728 for the HAp/60BNKT bioceramic. It should be noted that the ε_r for this HAp/60BNKT bioceramic ($\varepsilon_{max} \sim$ 230.28) is higher than the values from many previous work for the HAp/60BT composites, which had the ε_r of 100–125 [42, 43]. Vouilloz et al [42] also observed similar behavior in the increasing relative permittivity or ε_r value as an increasing $BaTiO_3$ piezoelectric phase. Since the increasing percentage of BNKT caused the reduction number of pores in the microstructure, and the sample density plays a role in the dielectric

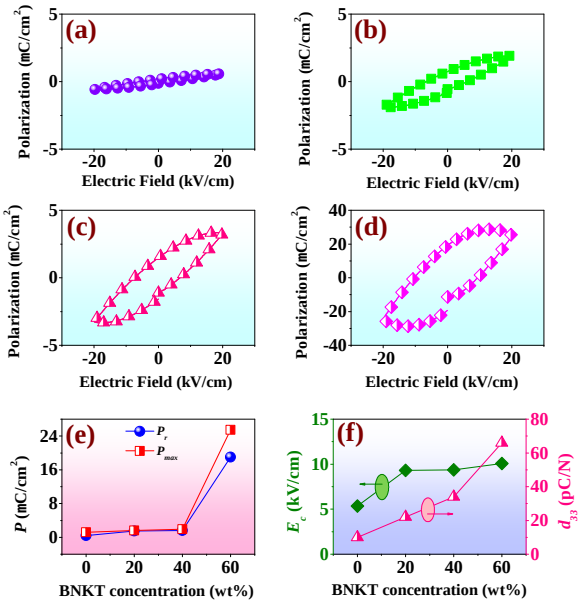

Fig. 5 Polarization-electric field (*P*-*E*) hysteresis loops of the HAp/xBNKT bioceramics, measured under an electric field of 20 kV/cm and a frequency of 1 Hz, (a) HAp, (b) HAp/20BNKT, (c) HAp/40BNKT, (d) HAp/60BNKT, (e) the P_{max} and P_r values as a function of BNKT content, and (f) the E_c and d_{33} values as a function of BNKT content.

constant variation [12]. The improvement of the dielectric performance with increasing BNKT content in this work can be linked with many facts that lower porosity, higher BNKT piezoelectric phase (higher interaction between piezoelectric phases), and higher density could produce the higher polarization for the studied bioceramics [15, 22].

Ferroelectric and piezoelectric analysis

Polarization-electric field (*P*-*E*) hysteresis loops of the HAp/xBNKT bioceramics, measured under an electric field of 20 kV/cm and a frequency of 1 Hz are shown in Fig. 5(a–d). The related ferroelectric values are also summarized in Table 2. The P_{max}, P_r, and E_c values as a function of BNKT content were also presented in Fig. 5(e,f). The *P*-*E* loop for the pure HAp bioceramic displayed a very small and slant hysteresis loop with the minimum values of P_{max} = 1.22 μC/cm^2, P_r = 0.43 μC/cm^2, and E_c = 5.35 kV/cm. With increasing BNKT content, however, the *P*-*E* loops presented an improvement of ferroelectric behavior with typical ferroelectric hysteresis loops, especially, the HAp/60BNKT bioceramic had the maximum values of P_{max} = 25.46 μC/cm^2, P_r = 18.99 μC/cm^2, and E_c = 10.08 kV/cm. The P_{max}, P_r and E_c values increased with increasing BNKT content as expected because the BNKT ceramic possessed a strong ferroelectricity. Therefore, the improvement of ferroelectric is affected by the amount of the BNKT piezoelectric phase as similar to previous reports [21, 22].

Piezoelectric behavior of the sintered bioceramics can be described with the evaluation of the piezoelectric coefficient or d_{33} value. This parameter can be related to microstructure features, crystalline phase distribution, and the densification degree [42]. The properties of the piezoelectric composites also depends, to a large extent, on the amount of piezoelectric ceramics they contain, which is a design parameter to be optimized for end applications [43, 44]. Therefore, the effect of BNKT content on the piezoelectric properties of the bioceramics was studied in detail for this work. The d_{33} value as a function of BNKT content at RT of the studied bioceramics is shown in Fig. 5(f). The d_{33} also showed a similar trend to that of the ε_r and P_r values. The pure HAp bioceramic had d_{33} of 10 pC/N. The measured d_{33} increased with increasing BNKT concentration and showed a maximum value of 66 pC/N for the HAp/60BNKT bioceramic. It should be noted that the measured d_{33} value for the HAp/60BNKT bioceramic ($d_{33} \sim 60$ pC/N) in this work is higher than values from the previous work for the HA/BT composites ($d_{33} < 25$ pC/N) at the same volume fraction [43, 45] and the 30HAp-70BTS (d_{33} = 23 pC/N) [46]. The improvement of d_{33} value in this work was attributed to higher of P_r value with increasing BNKT content. This can be explained by the thermodynamic theory of ferroelectric, which can be expressed as the equation [30]:

$$d_{33} = 2\varepsilon_{33}\varepsilon_0 Q_{11} P_r, \tag{6}$$

where P_r is the remnant polarization, ε_{33} is the material dielectric constant, ε_0 is the vacuum permittivity, and Q_{11} is the electrostrictive coefficient (a constant for perovskite materials). The d_{33} was proportional to the P_r value. The high d_{33} in this work is attributed to the maximum P_r, and the relatively large ε_r of the HAp/60BNKT bioceramics [47]. Thus, the d_{33} of the modified bioceramics strongly depends on the BNKT additive which had strong piezoelectric phase filler. On the other hand, the high porosity level shown in samples with low BNKT concentration impeded the polarization process using the direct current arrangement, whereby the d_{33} had lower values in the pure HAp and HAp/20BNKT bioceramics as expected [42].

In vitro apatite-forming ability or bioactivity

Bone-like apatite forming plays an important role in the formation of new bone because it serves as the transition and bonding layer between the implant material and new bone. The absorption of ions and proteins in the blood is beneficial to the adhesion of bone cells and provides a suitable surface for the growth of new tissue [45]. To confirm the *in vitro* apatite-forming ability evaluation or *in vitro* bioactivity test in this work, all HAp/xBNKT bioceramics were immersed in

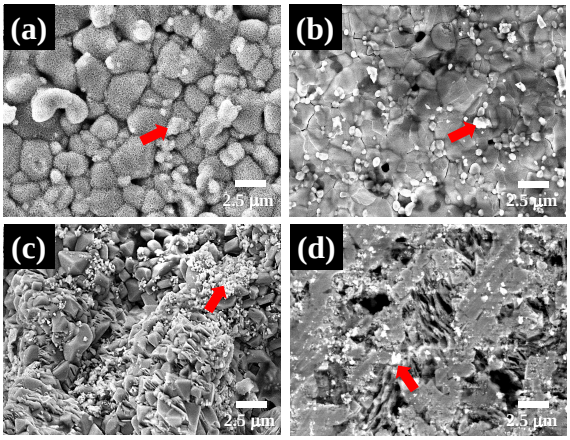

Fig. 6 SEM micrographs of the HAp/xBNKT bioceramics after being soaked in SBF solution for 21 days, (a) HAp, (b) HAp/20BNKT, (c) HAp/40BNKT, and (d) HAp/60BNKT (The red arrow "→" marked the small flakes of the apatite layer precipitated).

the SBF solution which is nearly equal to those in human blood plasma [48]. The SBF test is widely recognized for characterizing the *in vitro* bioactivity of a wide variety of materials. After 21 days of soaking in the SBF solution, all bioceramics were studied by SEM technique as the micrographs are shown in Fig. 6. SEM images clearly showed that the small flakes of the apatite layer precipitated and fully covered all surface areas for the pure HAp bioceramic. However, a few precipitated apatite crystals marked by the red arrow were observed on the surface of the BNKT-added bioceramics samples ($x = 20$, 40, and 60 wt%). Based on Fig. 6, the amount of apatite precipitated decreased with increasing BNKT content, where the apatite precipitates can be clearly seen for the samples contained BNKT $\leqslant$ 20 wt%. The reduction in apatite forming with increasing BNKT content indicated that BNKT phase has a lower apatite forming ability as compared to that of HAp phase. Tang et al [45] also reported that the apatite particles were deposited more on the HAp surface than the group that contained $BaTiO_3$ or the HAp-$BaTiO_3$ composites. This finding showed that the biocompatibility of the HAp was higher than that of the $BaTiO_3$. Normally, the HAp is the most widely investigated calcium phosphate biomaterial for the orthopaedic applications as it interacts with the host bone by exchanging Ca^{2+} and PO_4^{3-} ions. On exposure to the SBF sulution, the pure HAp surface naturally reveals a negative charge, and thereby interacts with positive calcium ions in the fluid to form the Ca-rich amorphous calcium phosphate (ACP) acquiring a positive charge. The Ca-rich ACP on the HAp relays the following electrostatic interaction with negative phosphate ions in the fluid to form the Ca-poor ACP, which eventually crystallizes into bone-like apatite [49]. This helps in stimulating the bone growth and enhanced the integration of the implant material with the host bone. Therefore, the pure HAp bioceramic is recognized as highly biocompatible and bioactive material when compared to that of the modified samples [15, 41]. On the other hand, it can be seen that the materials with more calcium phosphate have a recognized biocompatibility. In the assay, pure HAp and small BNKT- added bioceramics (BNKT $\leqslant$ 20 wt%), both compositions showed the expected behavior [42].

It can be observed that the HAp/60BNKT bioceramic had the lowest porosity, highest density, excellence mechanical and electrical performances than other compositions. Moreover, the HAp/60BNKT bioceramic also produced *in vitro* apatite precipitation and showed good bioactivity. Based on all the above results, this suggests that the HAp/60BNKT bioceramics are promising candidates for biomedical applications. In addition, further validation of the *in vitro* cell culture with cancer cells wound healing assays or inflammatory markers, and *in vivo* studies are needed to be performed in the future to confirm the findings of the current study.

CONCLUSION

In this work, the HAp/xBNKT bioceramics have been successfully synthesized by a solid-state mixed oxide method. The XRD analysis showed that the modified bioceramics have the mixed phases of HAp and BNKT. With increasing BNKT content, the improvement of densification, mechanical, and electrical properties were observed. The HAp/60BNKT bioceramics exhibited the maximum density, mechanical, dielectric, ferroelectric, and piezoelectric performances. *In vitro* bioactivity test suggested that the pure HAp bioceramic has a higher apatite-forming ability as compared to the BNKT-added bioceramics. Based on our results, these HAp/xBNKT bioceramics system had the potential to be a promising material candidate for biomedical applications.

Acknowledgements: This work was supported by the Fundamental Fund 2026, Rajamangala University of Technology Lanna (RMUTL) and the NSRF via the Program Management Unit for Human Resources & Institutional Development, Research and Innovation [B05F640198]. We thank the Department of Industrial Engineering, Materials and Medical Innovation Research Unit, Materials and Manufacturing Research Center, and Faculty of Engineering of RMUTL. The Department of Physics and Materials Science, Center of Excellence in Materials Science and Technology, Materials Science Research Center, Faculty of Science, and the Office of Research Administration, Chiang Mai University are also acknowledged.

REFERENCES

1. Panda S, Biswas CK, Paul S (2021) A comprehensive review on the preparation and application of cal-

cium hydroxyapatite: A special focus on atomic doping methods for bone tissue engineering. *Ceram Int* **47**, 28122–28144.
2. Arokiasamy P, Abdullah MMAB, Rahim SZA, Luhar S, Sandu AV, Jamil NH, Nabiałek M (2022) Synthesis methods of hydroxyapatite from natural sources: A review. *Ceram Int* **48**, 14959–14979.
3. Sari YW, Tsalsabila A, Darmawan N, Herbani Y (2022) Hydroxyapatite formation under calcium-deficient concentration conditions modulated by amino acid-capped gold nanoparticles. *Ceram Int* **48**, 13665–13675.
4. Rizkiana MF, Salsabila ZA, Aulia RI, Amini HW, Palupi B, Rahmawati I, Fachri BA (2024) Microwave-assisted synthesis of chitosan-hydroxyapatite composite from eggshells and its adsorption properties. *ScienceAsia* **50**, ID 2024067.
5. Alshemary AZ, Hussain R, Dalgic AD, Evis Z (2022) Bactericidal and *in vitro* osteogenic activity of nano sized cobalt-doped silicate hydroxyapatite. *Ceram Int* **48**, 28231–28239.
6. Ferreira CRD, Santiago AAG, Vasconcelos RC, Paiva DFF, Pirih FQ, Araújo AA, Motta FV, Bomio MRD (2022) Study of microstructural, mechanical, and biomedical properties of zirconia/hydroxyapatite ceramic composites. *Ceram Int* **48**, 12376–12386.
7. Jaita P, Jarupoom P (2023) Enhanced magnetic performance and *in vitro* apatite-forming ability of the $CoFe_2O_4$ doped nano-hydroxyapatite porous bioceramics. *Microsc Res Tech* **86**, 882–897.
8. Anandan D, Jaiswal AK (2024) Synthesis methods of hydroxyapatite and biomedical applications: An updated review. *J Aus Ceram Soc* **60**, 663–679.
9. Jiao H, Zhao K, Bian T, Tang Y (2017) Hydrothermal synthesis and properties characterization of barium titanate/hydroxyapatite spherical nanocomposite materials. *J Alloys Compd* **715**, 73–82.
10. Seet SL (2009) Silicon-substituted calcium phosphate compounds: Synthesis, characterization, and bioactivity evaluation. *ScienceAsia* **35**, 255–260.
11. Faksawat K, Limsuwan P, Naemchanthara K (2021) 3D printing technique of specific bone shape based on raw clay using hydroxyapatite as an additive material. *Appl Clay Sci* **214**, 106269.
12. Ibrahim KE, Kassim HA (2023) Investigation of structural, dielectric, impedance, and mechanical properties of hydroxyapatite modified barium titanate composites for biomedical applications. *Open Chem* **21**, 20230140.
13. Bowen CR, Gittings J, Turner IG, Baxter F, Chaudhuri JB (2006) Dielectric and piezoelectric properties of hydroxyapatite-$BaTiO_3$ composites. *Appl Phys Lett* **89**, 132906.
14. Liu B, Chen L, Shao C, Zhang F, Zhou K, Cao J, Zhang D (2016) Improved osteoblasts growth on osteomimetic hydroxyapatite/$BaTiO_3$ composites with aligned lamellar porous structure. *Mater Sci Eng C* **61**, 8–14.
15. Verma AS, Kumar D, Dubey AK (2019) Dielectric and electrical response of hydroxyapatite-$Na_{0.5}K_{0.5}NbO_3$ bioceramic composite. *Ceram Int* **45**, 3297–3305.
16. Linh NTB, Mondal D, Lee BT (2014) In vitro study of $CaTiO_3$-hydroxyapatite composites for bone tissue engineering. *ASAIO J* **60**, 722–729.
17. Jarkov V, Allan SJ, Bowen C, Khanbareh H (2022) Piezoelectric materials and systems for tissue engineering and implantable energy harvesting devices for biomedical applications. *Int Mater Rev* **67**, 683–733.
18. Jacob J, More N, Kalia K, Kapusetti G (2018) Piezoelectric smart biomaterials for bone and cartilage tissue engineering. *Inflamm Regen* **38**, 1–11.
19. Sasaki A, Chiba T, Mamiya Y, Otsuki E (1999) Dielectric and piezoelectric properties of $(Bi_{0.5}Na_{0.5})TiO_3$-$(Bi_{0.5}K_{0.5})TiO_3$ systems. *Jpn J Appl Phys* **38**, 5564–5567.
20. Parjansri P, Kamlangkla K, Eitssayeam S, Inthata U (2025) The influence of $BaTiO_3$ nanocrystals on the electrical characteristics and energy storage capabilities of BNKT ceramics. *J Sci Adv Mater Devices* **10**, 100918.
21. Jaita P, Watcharapasorn A, Cann DP, Jiansirisomboon S (2014) Dielectric, ferroelectric and electric field-induced strain behavior of $Ba(Ti_{0.90}Sn_{0.10})O_3$-modified $Bi_{0.5}(Na_{0.80}K_{0.20})_{0.5}TiO_3$ lead-free piezoelectrics. *J Alloys Compd* **596**, 98–106.
22. Jaita P, Watcharapasorn A, Kumar N, Jiansirisomboon S, Cann DP (2016) Lead-free $(Ba_{0.70}Sr_{0.30})TiO_3$-modified $Bi_{0.5}(Na_{0.80}K_{0.20})_{0.5}TiO_3$ ceramics with large electric field-induced strains. *J Am Ceram Soc* **99**, 1615–1624.
23. Jaita P, Chokethawai K, Randorn C, Boonsri K, Pringproa K, Thongkorn K, Watcharapasorn A, Jarupoom P (2024) Enhancing bioactivity and mechanical performances of hydroxyapatite-calcium sulfate bone cements for bone repair: *in vivo* histological evaluation in rabbit femurs. *RSC Adv* **14**, 23286.
24. Antis GR, Chantikul P, Lawn BR, Marshall DB (1981) A critical evaluation of indentation techniques for measuring fracture toughness: I, direct crack measurement. *J Am Ceram Soc* **64**, 533–538.
25. Jarupoom P, Jaita P (2015) Influence of barium hexaferrite on magnetic properties of hydroxyapatite ceramics. *J Nanosci Nanotechnol* **15**, 9217–9221.
26. Meema HE, Meema S (1978) Compact bone mineral density of the normal human radius. *Acta Radiol Oncol Radiat Phys Biol* **17**, 342–352.
27. Mohammad NF, Kanesvaran G, Othman SM, Mohammad IS (2012) Effect of particulate size on mechanical strength of anadara granosa bioceramic. In: *International Conference on Biomedical Engineering (ICoBE)*, Penang.
28. Zhang YR, Li JF, Zhang BP (2008) Enhancing electrical properties in NBT-KBT lead-free piezoelectric ceramics by optimizing sintering temperature. *J Am Ceram Soc* **91**, 2716–2719.
29. Yoon SH, Kwon SH, Hur KH (2011) Dielectric relaxation behavior of acceptor (Mg)-doped $BaTiO_3$. *J Appl Phys* **109**, 084117.
30. Jaita P, Manotham S, Butnoi P, Sanjoom R, Arkornsakul P, Sweatman DR, Kruea-In C, Tunkasiri T (2018) The mechanical and electrical properties of modified-BNKT lead-free ceramics. *Int Ferroelectrics* **187**, 147–155.
31. Ghorbal GB, Tricoteaux A, Thuault A, Louis G, Chicot D (2017) Comparison of conventional Knoop and Vickers hardness of ceramic materials. *J Eur Ceram Soc* **37**, 2531–2535.
32. Strecker K, Ribeiro S, Hoffmann MJ (2005) Fracture toughness measurements of LPS-SiC: A Comparison of the indentation technique and the SEVNB method. *Mater Res* **8**, 121–124.
33. Hussein R, Landon Y, Araujo AC (2023) *Bone Properties*, COBEF2023, Brasilia, Brazil.

34. Roy ME, Rho JY, Tsui TY, Evans ND, Pharr GM (1999) Mechanical and morphological variation of the human lumbar vertebral cortical and trabecular bone. *J Biomed Mater Res* **44**, 191–197.
35. Kruea-In C, Inthong S, Leenakul W (2017) Effects of NiO nanoparticles on physical and mechanical properties of BNKT lead-free ceramics. *Appl Mech Mater* **866**, 282–286.
36. Callister WD, Rethwisch DG (2003) *Materials Science and Engineering: An Introduction*, John Wiley & Sons Inc, New York.
37. Hoepfner TP, Case ED (2003) The influence of the microstructure on the hardness of sintered hydroxyapatite. *Ceram Int* **29**, 699–706.
38. Chang CI, Lee CJ, Huang JC (2004) Relationship between grain size and Zener-Holloman parameter during friction stir processing in AZ31 Mg alloys. *Scr Mater* **51**, 509–514.
39. Jaita P, Jarupoom P (2021) Enhanced dielectric, piezoelectric, and mechanical performances of barium strontium titanate-modified $(Bi_{0.487}Na_{0.487}La_{0.017})TiO_3$ lead-free ceramics. *Int Ferroelectrics* **213**, 209–220.
40. Nayak B, Misra PK (2020) Exploration of the structural and dielectric characteristics of a potent hydroxyapatite coated gallium bioceramics for the forthcoming biomedical and orthopedic applications. *Mater Chem Phys* **239**, 121967.
41. Dubey AK, Basu B, Balani K, Guo R, Bhalla AS (2011) Dielectric and pyroelectric properties of HAp-$BaTiO_3$ composites. *Ferroelectrics* **423**, 63–76.
42. Vouilloz FJ, Castro MS, Vargas GE, Gorustovich A, Fanovich MA (2017) Reactivity of $BaTiO_3$-$Ca_{10}(PO_4)_6(OH)_2$ phases in composite materials for biomedical applications. *Ceram Int* **43**, 4212–4221.
43. Gittings JP, Bowen CR, Turner IG, Baxter F, Chaudhuri J (2007) Characterisation of ferroelectric-calcium phosphate composites and ceramics. *J Eur Ceram Soc* **27**, 4187–4190.
44. Xin C, Shifeng H, Jun C, Zongjin L (2007) Piezoelectric, dielectric, and ferroelectric properties of 0-3 ceramic/cement composites. *J Appl Phys* **101**, 094110.
45. Tang Y, Wu C, Wu Z, Hu L, Zhang W, Zhao K (2017) Fabrication and *in vitro* biological properties of piezoelectric bioceramics for bone regeneration. *Sci Rep* **7**, 43360.
46. Uribe R, Rojas I, Riofrio MC, Lascano L, González G (2022) Polarization and biomineralization of hydroxyapatite-barium titanate composites. *J Phys Conf Ser* **2238**, 012007.
47. Ullah A, Ahn CW, Malik RA, Lee JS, Kim IW (2014) Electromechanical and microstructural study of $(1\text{-}x)Bi_{0.5}(Na_{0.80}K_{0.20})TiO_3$-$x(Ba_{0.70}Sr_{0.30})TiO_3$ lead-free piezoelectric ceramics. *J Electroceram* **33**, 187–194.
48. Zadpoor AA (2014) Relationship between *in vitro* apatite-forming ability measured using simulated body fluid and *in vivo* bioactivity of biomaterials. *Mater Sci Eng C* **35**, 134–143.
49. Kim HM, Himeno T, Kawashita M, Kokubo T, Nakamura T (2004) The mechanism of biomineralization of bone-like apatite on synthetic hydroxyapatite: An *in vitro* assessment. *J R Soc Interface* **1**, 17–22.